Published in final edited form as:
Adv Funct Mater. 2007 July 9; 17(10): 1645–1653. doi:10.1002/adfm.200600669.

Micropatterned Polypyrrole: A Combination of Electrical and Topographical Characteristics for the Stimulation of Cells**

Natalia Gomez [Dr.],
Department of Chemical Engineering, The University of Texas at Austin, Austin, TX 78712-1062 (USA)

Jae Y. Lee,
Department of Chemical Engineering, The University of Texas at Austin, Austin, TX 78712-1062 (USA)

Jon D. Nickels, and
Department of Biomedical Engineering, The University of Texas at Austin, Austin, TX 78712-1062 (USA)

Christine E. Schmidt [Prof]
Department of Chemical Engineering, The University of Texas at Austin, Austin, TX 78712-1062 (USA)

Department of Biomedical Engineering, The University of Texas at Austin, Austin, TX 78712-1062 (USA)

Texas Materials Institute, The University of Texas at Austin, Austin, TX 78712-1062 (USA)

Center for Nano- and Molecular Science and Technology, The University of Texas at Austin, Austin, TX 78712-1062 (USA)

Natalia Gomez: ; Jae Y. Lee: ; Jon D. Nickels: ; Christine E. Schmidt: schmidt@che.utexas.edu

Abstract

Electrically conducting polymers such as polypyrrole (PPy) are important biomaterials in neural engineering applications, including neural probes, nerve conduits, and scaffolds for tissue and nerve regeneration. Surface modification of these polymers can introduce other valuable characteristics for neural interfacing in addition to electrical conductivity, such as topographical features and chemical bioactivity. Here, the patterning of PPy to create topographical cues for cells is reported. In particular, 1 and 2 μm wide PPy microchannels are fabricated using electron-beam (e-beam) lithography and electropolymerization. A systematic analysis of parameters controlling PPy micropatterning is performed, and finds that microchannel depth, roughness, and morphology are highly dependent on the e-beam writing current, polymerization current, PPy/dopant concentrations, and the polymerization time. Embryonic hippocampal neurons cultured on patterned PPy polarize (i.e., defined an axon) faster on this modified material, with a twofold increase in the number of cells with axons compared to cells cultured on unmodified PPy. These topographical features also have an effect on axon orientation but do not have a significant effect on overall axon length. This is the first investigation that studies controlled PPy patterning with small dimensions (i.e., less than 5 μm) for

**Funding for this work was provided by grants from the Gillson Longenbaugh Foundation and NIH (R01 EB004529). We thank the Welch Foundation and SPRING for partial financial support in the CNM facilities. We acknowledge Maeve Cooney's assistance with manuscript and figure editing.

Correspondence to: Christine E. Schmidt, schmidt@che.utexas.edu.

biological applications, which demonstrates the relevance of expanding microelectronic materials and techniques to the biomedical field.

1. Introduction

Polypyrrole (PPy), a biocompatible electrically conductive polymer, is extensively used in biological applications such as neural electrodes,[1–3] and scaffolds for nerve regeneration in neural-tissue engineering.[4–6] PPy is an attractive material for neural probes and nerve guidance channels because of its biocompatibility, good conductivity, ease of synthesis, and the potential to have high surface areas.[3,7] However, it is still desired for these and other biomedical applications to provide additional chemical and physical guidance cues for cells, in conjunction with electroactivity provided by the conducting polymer.

Surface modification of conducting polymers for incorporating biological cues involves different approaches that impact chemical and physical properties of the polymer. Chemical modification has been extensively investigated using biomolecules as dopants,[8–10] or by immobilizing bioactive moieties on the surface of the material.[2,11–13] Physical modification has been explored by increasing surface roughness using various methods, such as creating microporous films using polystyrene sphere templates,[14] fabricating composites of nanoparticles and polylactide,[15] growing conducting polymers within hydrogels,[16] and blending with biomolecules to yield “fuzzy” structures.[8]

We recently reported covalent immobilization of nerve growth factor (NGF) on the surface of PPy.[17] Combination of this bioactive surface with electrical stimulation, provided by PPy, enhanced neurite extension. In a different study, poly(dimethyl siloxane) (PDMS) microchannels modified with immobilized NGF effectively increased neuronal polarization (i.e., axon formation) and the axon length of neurons.[18] Combination of physical cues (i.e., microchannels) and chemical guidance (i.e., immobilized protein) was essential for favorable neuronal responses. Based on these results, we hypothesize that a conducting polymer with both physical- and chemical-guidance cues could further improve axon formation and growth. Fabrication of PPy microchannels as described here provides both physical and electrical cues to neurons, which can be subsequently combined with immobilized NGF to further enhance neuronal behavior.

In an effort to modify PPy with topographical features, we report the fabrication of 1 and 2 μm wide microchannels using electron-beam (e-beam) lithography and electropolymerization. Although PPy patterning for microelectronic applications has been extensively reported in the literature,[19–29] patterns smaller than 5 μm (the relevant size for many cell functions) have been scarcely studied. More importantly, biological applications of small PPy patterns (i.e., less than 5 μm) have not been investigated. Additionally, there are no previous studies on the effect of patterning and polymerization techniques on pattern size (e.g., width and depth), morphology, and surface roughness—important parameters for cellular applications.

E-beam writing and polymerization conditions were found to drastically affect the morphology of the microchannels, determining the depth, roughness, and sharpness of the patterns. We investigated a range of electropolymerization conditions including monomer and dopant concentration (12.5–100 m_M), polymerization current (36–720 μA), and polymerization time. In cases of higher monomer concentrations, larger currents, and longer polymerization times, the channels were deeper and rougher, and the geometry and edges were less defined.

We investigated the effect of the fabricated PPy microchannels on the polarization and axon length of hippocampal cells, which have been used extensively in the past as a model system for this type of behavior of neurons.[30,31] Microchannels were shown to have a significant

effect on neuron polarization with a twofold increase in the number of neurons with axons, whereas the effect of topography on axon length is negligible. Microchannels also have an effect on the orientation of axon growth, promoting parallel or perpendicular alignment with respect to the microchannels. These novel results demonstrate that controlled PPy patterning with small dimensions can be applied to cellular and biomedical purposes, in addition to the traditional microelectronic applications.

2. Results and Discussion

2.1. Fabrication and Characterization of PPy Microchannels

PPy microchannels were fabricated by taking advantage of the electropolymerization process, in which the pyrrole monomer only polymerizes on substrates that are electrically conductive. This technique is widely used for performing polymer synthesis using a metal or indium tin oxide (ITO)-coated substrate.[32] Based on this principle, the fabrication of PPy microchannels was performed by first patterning an insulating resist on a conductive substrate using e-beam lithography, a direct-writing technique,[33] and then polymerizing on the exposed conductive areas (Fig. 1). Other techniques, such as patterning of self-assembled monolayers, can also be used to create insulating patterns on conductive substrates for patterning PPy.[22,23]

The growth and morphology of PPy microchannels was strongly dependent on electropolymerization conditions, in particular monomer and dopant concentrations, polymerization current, and time. All studied conditions are summarized in Table 1, which also includes the depth and gap width of the microchannels obtained from scanning electron microscopy (SEM) images of cross sections, and the roughness obtained from atomic force microscopy (AFM). As illustrated in Figure 2, Figure 3, and Figure 4, polymerization conditions determined the depth, roughness, and geometry of the structures. In general, for larger polymerization currents and higher monomer/dopant concentrations, such as in Figure 2A–C, microchannels polymerized rapidly producing deeper and rougher structures. These conditions also produced less-defined geometries, decreasing the gap distance between subsequent microchannels. For smaller polymerization currents and lower pyrrole/dopant concentrations, the reaction was more controlled, producing smoother PPy structures and maintaining the original dimensions of the ITO patterns. Figure 2 illustrates the growth trend for some of the studied conditions, which suggests a larger impact of the polymerization current on the microchannel depth. Figure 3B further illustrates that the combination of high concentration and high current ultimately produces the deepest microchannels. Figure 4 shows AFM images of microchannels under two different conditions, and of thin film controls, and illustrates the increase in roughness with increasing depth. This is the same trend previously reported for PPy thin films.[3]

PPy growth is controlled by electric-field properties (current or voltage) and solution concentration of monomer and electrolyte.[34,35] Low monomer concentration is known to result in diffusion-limited aggregation growth (i.e., nucleation-limited polymerization), whereas low voltages or currents result in diffusion- limited polymerization growth (i.e., growth-rate-limited polymerization).[34] Correspondingly, nucleation has been classified as instantaneous or progressive, and the growth as two or three dimensional.[36] Low monomer concentration produces fewer nuclei. When the current is also low, the nuclei grow slowly in two dimensions. On the contrary, high monomer concentration induces high nucleation, which is translated in the formation of many PPy particles on the substrate surface. High polymerization currents produce rapid growth of the nuclei in a three dimensional fashion. Combined low monomer concentration and low current produces few PPy nuclei that grow slowly in two dimensions (i.e., thin films, smooth surfaces). High monomer concentration and large current produces many nuclei that grow very rapidly in a three dimensional fashion (i.e.,

thick films, rough surfaces). These growth characteristics explain the obtained microchannel morphologies depending on the polymerization conditions.

E-beam writing current also affected PPy microchannel growth. Figure 5 shows patterns written with low currents, which exhibited slow growth. This difference could be a result of the subsequent poly(methyl methacrylate) (PMMA) resist development, which removes more or less material on the patterns depending on the exposure to the e-beam.[37] Lower current during the writing correlates with less development of the resist, which further translates to more PMMA-protected ITO areas, and therefore less polymerization.

In a similar way, PMMA resist thickness plays a role in the depth and morphology of the PPy microchannels, as observed in Figure 6. Figure 6A shows an SEM image of microchannels synthesized with a ca. 10 nm PMMA resist, whereas Figure 6B shows an image of microchannels synthesized with the same exact conditions as in Figure 6A (50 m_M pyrrole/poly (styrene sulfonate) (PSS) concentration and 144 μA), but with a PMMA resist ca. 100 nm. The thicker PMMA resist produced very clean, well-defined structures, without any additional PPy particles in the area surrounding the microchannels. In addition, microchannels are deeper on the thick PMMA (depth = (799.3 ± 113), and (338 ± 49) nm for 100 and 10 nm PMMA resist, respectively). This difference is probably a result of the higher insulating layer of the thick PMMA, which avoids polymerization of pyrrole on the coated areas, and therefore allows the structures to grow more easily without filling the spaces between the channels. These results suggest that e-beam variables could also be precisely tuned for controlling the conducting polymer patterns.

PPy micropatterning has been extensively explored for microelectronic applications, but not for biological applications. Microcontact printing techniques have been utilized in several applications for the patterning of silanes[19–22] and alkanethiols.[23,24] Patterned silanes can create positive or negative PPy patterns depending on the underlying substrate (pattern size ca. 15–50 μm).[19,22] Microcontact printing of aminosilanes has been used to pattern copper first, followed by PPy electrodeposition (pattern size ca. 2–80 μm).[21] Alkanethiols can be used for masking on a conductive substrate[23] (pattern size ca. 10 μm), or pyrrole–thiol compounds can be used to promote selective polymerization (pattern size ca. 2–10 μm).[24] Techniques such as conventional photolithography (pattern size ca. 30 μm),[25] domain separation of block copolymers (pattern size ca. 50 nm),[26] masking by polymer brushes (pattern size ca. 50 μm),[27] mold insertion (pattern size ca. 50–300 μm),[28] and photopolymerization (pattern size ca. 25 μm)[29] have also been explored for patterning PPy.

Many of these PPy patterning techniques have only created patterns with dimensions between 10 and 100 μm. In the present studies, e-beam lithography allowed patterning of structures on a scale relevant to cell function (< 5 μm). In addition, pattern depth and roughness are also important in the biomaterials field, which was not reported in many of these previous studies. We found that although e-beam writing is time-consuming, it allowed the fabrication of smaller patterns, in addition to better control over polymer growth by modulating the writing current and subsequent development of the resist.

More importantly, investigations of PPy micropatterning for influencing cell function are very limited. Song et al.[38] reported the fabrication of PPy patterns (pattern size ca. 100 μm) to show the selective modification of PPy with adhesive molecules that influence cell adhesion. This larger-scale patterning could be used to control cell organization and positioning, whereas the techniques and dimensions described here are used to control axonal outgrowth more directly, which is fundamental for neural-engineering applications. In particular, patterning of conducting polymers such as PPy could be used in neural probes or nerve conduits to create surfaces that modulate neuron responses to the implanted device.

2.2. Hippocampal Neuron Response to PPy Microchannels

Embryonic hippocampal neurons were cultured on micro-structured and unmodified PPy to determine the effects of topography on polarization and axon elongation. One set of PPy patterning conditions was chosen for fabricating well-defined patterns for cell culture. These conditions were an e-beam current of 0.1 nA, electropolymerization with 25 mM pyrrole and PSS, 144 μA, and 30 s of polymerization.

We previously reported that 1–2 μm wide and 400–800 nm deep PDMS microchannels significantly increased the number of stage-3 cells (i.e., polarized neurons) during the first 20 h in culture.[18] Here, we corroborated and confirmed these results by fabricating similar topographical features on a conducting polymer. As observed in Figure 7, hippocampal neurons cultured on PPy microchannels polarized faster, meaning that more cells had defined axons compared to controls on unmodified PPy. Figure 8A illustrates the quantitative analysis of these responses. Both 1 and 2 μm microchannels had a statistically significant increase in the number of polarized cells with respect to cells on unpatterned PPy (probability, $P = 0.0007$ for 2 μm microchannels; $P = 0.009$ for 1 μm microchannels). Similar results on PDMS substrates are also shown in this graph, which further confirms the particular effect of the topography itself and not the specific material. It is important to mention that the surface roughness (root mean square; rms) of the thin film was ca. 19 nm, which is larger than the roughness of the microchannels (from Table 1, rms ~ 14 nm). These data eliminate the possibility that increased roughness and surface area enhanced neuron polarization for the PPy microchannels.

Others have also observed the effect of material topography on neuron polarization. Dowell-Mesfin et al. showed that silicon pillars of 2 μm width increased the number of cells in stage 3 after 24 h in culture,[39] but quantitative measurements were not reported. More recently, Foley et al. showed increased neuritogenesis on nanoridges in PC12 cells (rat pheochromocytoma cells: a neuronlike cell line) with low levels of NGF,[40] and Ahmed et al. reported an increase in neurite generation in several neuronal types cultured on nanofibers.[41] These responses to topography are thought to be transduced by tension generated within the cytoskeleton and the redistribution of focal adhesion complexes (FAC) as a result of the patterns.[42] Additionally, the cytoskeleton is directly connected to the nuclear membrane that ultimately alters nuclear morphology, which has been hypothesized to be connected to changes in gene expression.[42,43]

Axonal length of neurons was also investigated. Figure 8B shows that PPy microtopography did not result in a significant increase in axon length from hippocampal cells compared to cells cultured on unmodified PPy ($P = 0.13$ for 2 μm microchannels; $P = 0.92$ for 1 μm microchannels). We previously found this same trend on PDMS microchannels,[18] as illustrated in Figure 8B. These results suggest that surface topographical features have a more dramatic effect on axon-initiation mechanisms (i.e., polarization), but these effects become negligible once the axon is established and undergoes elongation. In contrast, we previously reported that ligands such as NGF have a stronger effect on axon elongation than topography.[18] This trend suggests that physical guidance provided by PPy microchannels could be combined with chemical cues such as immobilized NGF to further optimize axon outgrowth.

Axon orientation was analyzed by determining the angle of growth with respect to the direction of the microchannels. Figure 9 shows a tendency for axons to grow either in a perpendicular (90°) or parallel orientation (0° or 180°) with respect to 2 μm microchannels. Axon orientation on 1 μm PPy microchannels did not show any significant trend, which diverges from the perpendicular orientation observed on 1 μm PDMS microchannels.[18] We hypothesize that less-well-defined PPy microchannel morphology and geometry compared to PDMS resulted in lower orientation bias in the cells. Although we did not explore additional dimensions for

cell studies, increased axon alignment is expected with increasing depth and gaps between microchannels.

3. Conclusions

We have investigated neuron polarization, axon length, and orientation on microstructured PPy. For this, 1 and 2 μm wide microchannels were patterned on ITO-coated slides using e-beam lithography and electropolymerization. We found that PPy microchannel morphology depended strongly both on the e-beam writing and the electropolymerization conditions, producing deeper, less-defined, and rougher structures for higher e-beam writing currents, higher electropolymerization currents, higher pyrrole/dopant concentrations, and increasing polymerization times. A larger number of neurons cultured on patterned PPy polarized more readily, meaning that more cells had defined axons after 20 h in culture compared to unmodified PPy substrates (a twofold increase). The effect of topography on axon length was found to be negligible, which is consistent with data on PDMS microchannels.[18] These PPy microchannels could be further modified with immobilized NGF as we previously published, [17] to take full advantage of multiple cues to stimulate cells. This modified PPy could be potentially applied in neural tissue engineering applications such as neural probes and nerve conduits.

4. Experimental

Microfabrication of PPy Channels

Microchannels 1 and 2 μm wide and 50–2000 nm deep were created on PPy using microfabrication techniques. The procedure had two steps: 1) patterning the resist using e-beam lithography, and 2) electropolymerization of PPy on the patterns (see Fig. 1).

Micropatterns were written with e-beam lithography. ITO (a conducting material) coated glass slides (Delta Technologies) were cut into 4 cm^2 pieces and spin-coated with 1% PMMA resist in anisole (Microchem) for 45 s and 3000 rpm, and baked for 1 h at 160 °C. Microchannels of 1 or 2 μm were written on the PMMA resist using an e-beam (Raith-50 and XL-30 scanning electron microscopes, LaB_6 source) with an area dose of 220 μ A s cm^{-2} and beam current of 0.1 nA. After the patterns were written, electron-exposed areas were developed with a mixture of methylisobutylketone and isopropyl alcohol (1:3) (Sigma) for 1 min, followed by 1 min in isopropyl alcohol, exposing the conducting ITO on those areas. For thick-resist experiments, 2% PMMA resist in chlorobenzene was spin-coated with the same conditions.

PPy microchannels were polymerized electrochemically, a common technique to synthesize PPy thin films [4]. Patterned ITO coated slides were used for the galvanostatic deposition of the conducting polymer. Specifically, a three-electrode cell was used, which consisted of the ITO slide as the working electrode, a platinum-gauze counter electrode, and a saturated calomel reference electrode. The polymer was deposited from an aqueous solution of 12.5–100 mM pyrrole monomer (Aldrich) and 12.5–100 mM sodium salt of PSS (Aldrich), using an offset voltage of 720 mV and currents of 36–720 μA (see Table 1). A Pine Instruments AFRDE5 bipotentiostat was used as the dc voltage source. Microchannels were polymerized for 10 or 30 s as stated in Table 1.

Synthesis of PPy Thin Films (Unmodified PPy Controls)

PPy thin films were synthesized without patterns as controls for cell-culture studies. Thin films were electrochemically synthesized on plain ITO-coated slides with the same three-electrode cell used for PPy microchannels, using an aqueous solution of 25 mM pyrrole monomer and 25 mM PSS, an offset voltage of 720 mV, and a current of 7.2 mA. Higher polymerization current

and time were required to polymerize thin films, as the area available for polymerization was much larger (ca. 6 cm × 2 cm) than for samples with microchannels. Thin films were subsequently cut in 1 cm^2 pieces, and used for cell culture.

Microfabrication of PDMS Channels

Microchannels 1 and 2 μm wide and 400 nm deep were created on PDMS using soft-lithography techniques as previously described, and used here as controls [18]. Briefly, e-beam lithography was used to write patterns on 4% PMMA resist in chlorobenzene (Microchem), which was spin-coated on silicon wafers with a 4 μm thick SiO_2 layer. After writing and development, lift-off was performed by using thermal evaporation (Denton) of a 100 nm chromium film (R. D. Mathis) and acetone stripping. Reactive ion etching (RIE) of the SiO_2 layer was performed in an etcher (Plasma Technology) with a mixture of CHF_3 and oxygen. The etched wafer was silanized with tridecafluoro-1,1,2,2-(tetrahydrooctyl)trichlorosilane (Gelest), and subsequently used as a master for replica molding of the PDMS (Sylgard 184, Dow Corning) substrates. PDMS substrates with microchannels were coated with a layer of photoreactive polyallylamine as previously described [18], which rendered the material cell-adhesive for hippocampal neuron culture.

Hippocampal Cell Culture and Immunochemistry

For cell culture, PPy substrates (microchannels and thin films) were subsequently transferred to sterile 3 cm tissue culture dishes, UV-sterilized, incubated with poly-D-lysine (Sigma) for 2 h, washed twice with sterile water, air dried, and stored at 4 °C. Embryonic rat hippocampal cells (E18) were isolated from commercially obtained hippocampus tissue (BrainBits). The hippocampi were incubated with papain (Worthington) in Hibernate E medium (BrainBits) (4 mg mL^{-1}) at 30 °C for 20 min, followed by physical trituration with a fire-polished Pasteur pipette. Cells were counted and plated on PPy substrates at 7.5×10^3 cells cm^{-2}, and cultured with Neurobasal Medium (Invitrogen) supplemented with 2% B-27 (Invitrogen), L-glutamine (0.5 mM, Fisher), L-glutamic acid (25 μM, Sigma), and 1% antibiotic-antimycotic (10 000 units mL^{-1} of penicillin, 10 mg mL^{-1} of streptomycin, and 25 μg mL^{-1} of amphotericin, Sigma).

Cells were incubated on substrates with PPy microchannels and PPy thin films as controls. After 20 h in culture at 37 °C and 5% CO_2, cells were fixed with 4% paraformaldehyde (Sigma), 4% sucrose (Fisher) in PBS for 20 min, followed by permeabilization for 20 min with 0.1% Triton-X100 (Sigma) in 2% bovine serum albumin (BSA) (Jackson ImmunoResearch) in phosphate-buffered saline (PBS) (which we call PBS–BSA), and blocking for 1 h at 37 °C with 2% PBS–BSA. Samples were incubated with an antibody for Tau-1 (an axonal marker) (Chemicon, 1:200) in 2% PBS–BSA overnight at 4 °C, followed by incubation with a fluorescently labeled secondary antibody (Alexa 488-conjugated goat antimouse, Molecular Probes) for 1 h at 37 °C. Fluorescence images were captured with an inverted phase-contrast and fluorescence microscope (IX-70, Olympus), using a color CCD video camera (Optronics Magna- Fire, model S60800) and analyzed using Image J software (NIH). All cell experiments were repeated five times on different days. Experiments on PDMS substrates were performed following the same protocol.

Polarization and Axon-Length Analysis

Based on published criteria, a hippocampal cell was defined as polarized (stage 3) when one of its neurites was at least twice as long as the other neurites and it stained positively for Tau-1 [31,44,45]. The fraction of polarized cells was defined as the ratio of cells with axons to the total number of cells per sample as analyzed from fluorescence images. In the same experiments, axon length and angle were also measured and defined as the straight-line distance from the tip of the axon to the junction between the cell body and axon base, and the angle between this line and a 0° line in the direction of the microchannels (see inset in Fig. 5C). In

the case of branched axons, the length of the longest branch was measured from the tip of the axon to the cell body, and then each branch was measured from the tip of the axon to the branch point. An average of 100 cells were analyzed per sample and five samples were analyzed for each condition. The average and standard error of the mean (sem) were calculated for all data. *P* values for the fraction of polarized cells and axon-length data were analyzed using a 2-sided Student's t-test with respect to controls on PPy films. Statistical significance was determined for $P < 0.05$.

Scanning Electron Microscopy

Microchannel characteristics (channel depth and width) and axon extension were analyzed with a LEO 1530 scanning electron microscope. In particular, SEM, versus AFM, was used as a time-efficient technique to analyze a large number of samples for many different conditions, and thus to assess a general trend in microchannel properties as a result of several different processing parameters. Microchannels were imaged with a typical acceleration voltage of 10 kV. Microchannel depth and gap width were determined from SEM images by analyzing cross sections of the patterns (number of samples, $n = 3$). For imaging neurons, cells were fixed with 4% paraformaldehyde (Aldrich) and 4% sucrose in PBS for 20 min, and dehydrated with increasing concentrations of ethanol (30–100%) for a total time of 2 h, followed by 5 min exposure to hexamethyldisilazane (Sigma). After drying, samples were sputter-coated with a gold layer for SEM measurement and imaged with a typical acceleration voltage of 1 kV.

Atomic Force Microscopy

AFM images were acquired using an Asylum Research MFP-3D atomic force microscope for measuring PPy surface roughness. Standard silicon nitride cantilevers, model OTR8 (Veeco Nanoprobe), were used in contact mode at a scan rate of 0.5 Hz. 512 × 512 scans of 2 μm ×2 μm sections on top of the PPy channels were used for calculating rms surface roughness using MFP-3D software written in Igor Pro 5 (WaveMetrics Inc.). Larger overview scans (50 μm × 50 μm) were also acquired with 512 × 512 resolution with a 0.5 Hz scan rate.

References

1. George PM, Lyckman AW, LaVan DA, Hedge A, Leung Y, Avasare R, Testa C, Alexander PM, Langer R, Sur M. Biomaterials 2005;26:3511. [PubMed: 15621241]
2. Cui X, Wiler J, Dzaman M, Altschuler RA, Martin DC. Biomaterials 2003;24:777. [PubMed: 12485796]
3. Cui X, Hetke JF, Wiler JA, Anderson DJ, Martin DC. Sens. Actuators A 2001;93:8.
4. Schmidt CE, Shastri VR, Vacanti JP, Langer R. Proc. Natl. Acad. Sci. USA 1997;94:8948. [PubMed: 9256415]
5. Williams RL, Doherty PJ. J. Mater. Sci. Mater. Med 1994;5:429.
6. Chen SJ, Wang DY, Yuan CW, Wang XD, Zhang P, Gu XS. J. Mater. Sci. Lett 2000;19:2157.
7. Wang X, Gu X, Yuan C, Chen S, Zhang P, Zhang T, Yao J, Chen F, Chen G. J. Biomed. Mater. Res. A 2004;68:411. [PubMed: 14762920]
8. Cui X, Lee VA, Raphael Y, Wiler JA, Hetke JF, Anderson DJ, Martin DC. J. Biomed. Mater. Res 2001;56:261. [PubMed: 11340598]
9. Collier JH, Camp JP, Hudson TW, Schmidt CE. J. Biomed. Mater. Res 2000;50:574. [PubMed: 10756316]
10. Stauffer WR, Cui XT. Biomaterials 2006;27:2405. [PubMed: 16343612]
11. Cen L, Neoh KG, Li Y, Kang ET. Biomacromolecules 2004;5:2338.
12. De Giglio E, Sabbatini L, Colucci S, Zambonin G. J. Biomater. Sci. Polym. Ed 2000;11:1073. [PubMed: 11211158]
13. Sanghvi A, Miller KP, Belcher AM, Schmidt CE. Nat. Mater 2005;4:496. [PubMed: 15895095]
14. Yang J, Martin DC. Sens. Actuators B 2004;101:133.

15. Shi G, Rouabhia M, Wang Z, Dao LH, Zhang Z. Biomaterials 2004;25:2477. [PubMed: 14751732]
16. Kim DH, Abidian M, Martin DC. J. Biomed. Mater. Res. A 2004;71:577. [PubMed: 15514937]
17. Gomez N, Schmidt CE. J. Biomed. Mater. Res. A 2007;81:135. [PubMed: 17111407]
18. Gomez N, Lu Y, Chen S, Schmidt CE. Biomaterials 2007;28:271. [PubMed: 16919328]
19. Zhou F, Chen M, Liu W, Liu J, Liu Z, Mu Z. Adv. Mater 2003;15:1367.
20. Huang Z, Wang PC, Feng J, MacDiarmid G. Synth. Met 1997;85:1375.
21. Hale PS, Kappe P, Brack N, Prissanaroon W, Pigram PJ, Liesesang J. Appl. Surf. Sci 2006;252:2217.
22. Zhou F, Liu Z, Yu B, Chen M, Hao J, Liu W, Xue Q. Surf. Sci 2004;561:1.
23. Collard DM, Sayre CN. Synth. Met 1997;84:329.
24. Grace AN, Pandian K. J. Solid State Electrochem 2003;7:296.
25. Smela E, Gadegaard N. J. Phys. Chem. B 2001;105:9395.
26. Seo I, Pyo M, Cho G. Langmuir 2002;18:7253.
27. Zhou F, Liu W, Hao J, Xu T, Chen M, Xue Q. Adv. Funct. Mater 2003;13:938.
28. Luo C, Poddar R, Liu X. J. Vac. Sci. Technol. B 2006;24:L19.
29. Bai JB, Snively CM, Delgass WN, Lauterbach J. Adv. Mater 2002;14:1546.
30. Dotti CG, Sullivan CA, Banker GA. J. Neurosci 1988;8:1454. [PubMed: 3282038]
31. Fukata Y, Kimura T, Kaibuchi K. Neurosci. Res 2002;43:305. [PubMed: 12135774]
32. Diaz AF, Castillo JI, Logan JA, Lee WY. J. Electroanal. Chem 1981;129:115.
33. Norman JJ, Desai TA. Ann. Biomed. Eng 2006;34:89. [PubMed: 16525765]
34. Shan J, Yuan C, Zhang H. Thin Solid Films 1997;301:23.
35. Kaufman JH, Baker CK, Nazzal AI, Flickner M, Melroy OR. Phys. Rev. Lett 1986;56:1932. [PubMed: 10032814]
36. Hwang BJ, Santhanam R, Lin Y. J. Electrochem. Soc 2000;147:2252.
37. Madou, MJ. Fundamentals of Microfabrication. Vol. 2nd ed.. Boca Raton, FL: CRC Press; 2002.
38. Song HK, Toste B, Ahmann K, Hoffman-Kim D, Palmore GT. Biomaterials 2006;27:473. [PubMed: 16112728]
39. Dowell-Mesfin NM, Abdul-Karim MA, Turner AM, Schanz S, Craighead HG, Roysam B, Turner JN, Shain W. J. Neural Eng 2004;1:78. [PubMed: 15876626]
40. Foley JD, Grunwald EW, Nealey PF, Murphy CJ. Biomaterials 2005;26:3639. [PubMed: 15621254]
41. Ahmed L, Liu H, Mamiya P, Ponery AS, Babu AN, Weik T, Schindler M, Meiners S. J. Biomed. Mater. Res. A 2006;76:851. [PubMed: 16345089]
42. Dalby MJ. Med. Eng. Phys 2005;27:730. [PubMed: 15921949]
43. Dalby MJ, Riehle MO, Yarwood SJ, Wilkinson CD, Curtis AS. Exp. Cell Res 2003;284:274. [PubMed: 12651159]
44. Schwamborn JC, Puschel AW. Nat. Neurosci 2004;7:923. [PubMed: 15286792]
45. Menager C, Arimura N, Fukata Y, Kaibuchi K. J. Neurochem 2004;89:109. [PubMed: 15030394]

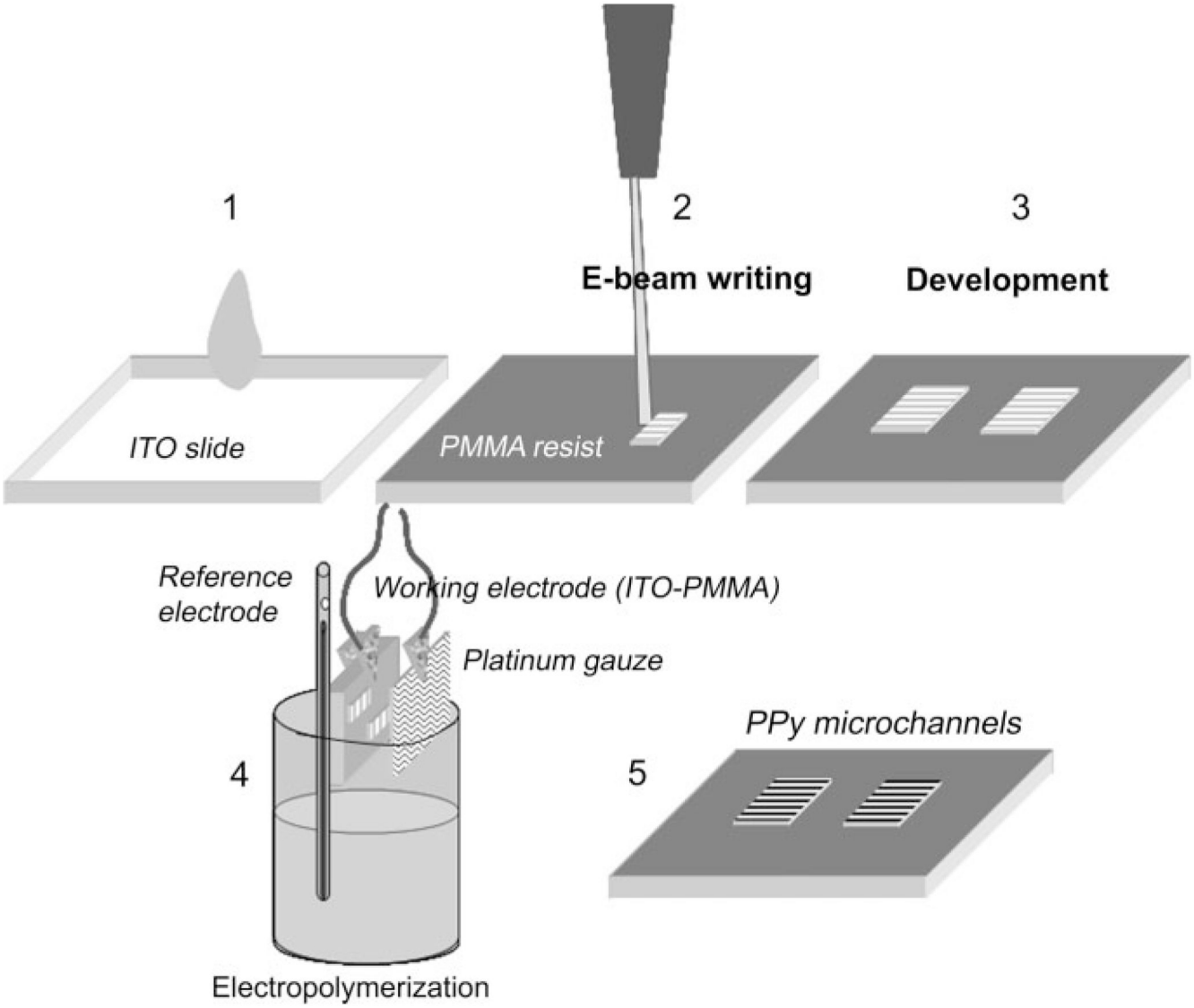

Figure 1.

A scheme for the fabrication of PPy microchannels. An ITO glass slide is spin-coated with a poly(methyl methacrylate) (PMMA) resist (1). Patterns are written using e-beam lithography (2), developed (3), and electropolymerized in a three-electrode cell with a pyrrole/PSS solution (4). PPy microchannels are created as PPy exclusively polymerizes on the developed conducting areas (5).

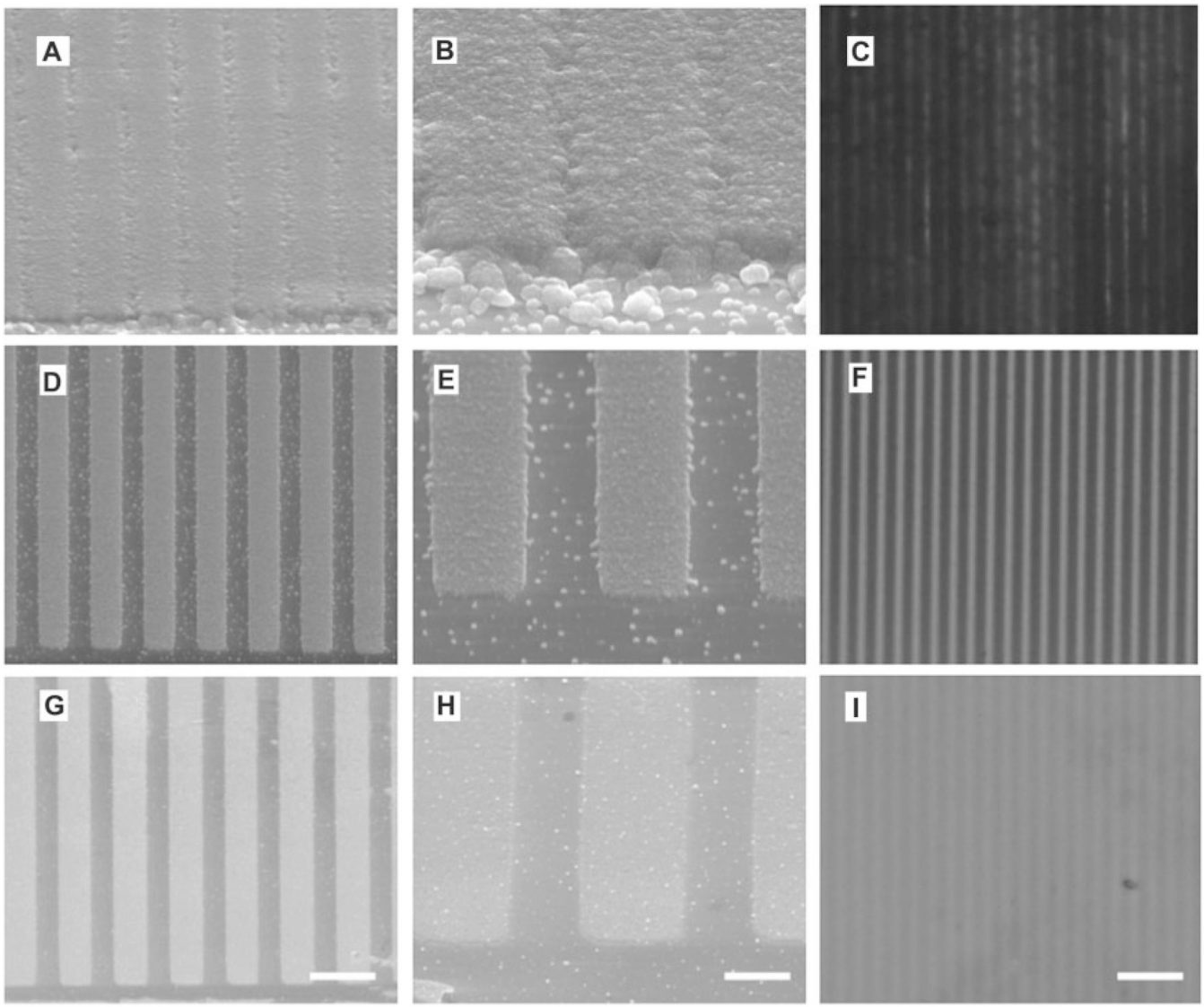

Figure 2.

PPy microchannel morphology for different electropolymerization conditions. A,B,D,E,G,H) SEM images and C,F,I) light microscopy images. Microchannels polymerized with A–C) 50 mM pyrrole/PSS concentration, 720 μA polymerization current, and 30 s of polymerization time (thickness ca. 900 nm); D–F) 25 mM pyrrole/PSS concentration, 144 μA polymerization current, and 30 s of polymerization time (thickness ca. 300 nm); G–I) 12.5 mM pyrrole/PSS concentration, 144 μA polymerization current, and 30 s of polymerization time (thickness ca. 50 nm). All patterns were written with 0.1 nA during e-beam lithography. SEM images show an increase in microchannel depth and roughness with increasing current and concentration. Light microscopy images show darker and less-defined structures for thicker microchannels. Polymerization conditions control microchannel depth, roughness, and morphology. The scale bar is 5 μm (A,D,G), 2 μm (B,E,H), and 10 μm (C,F,I).

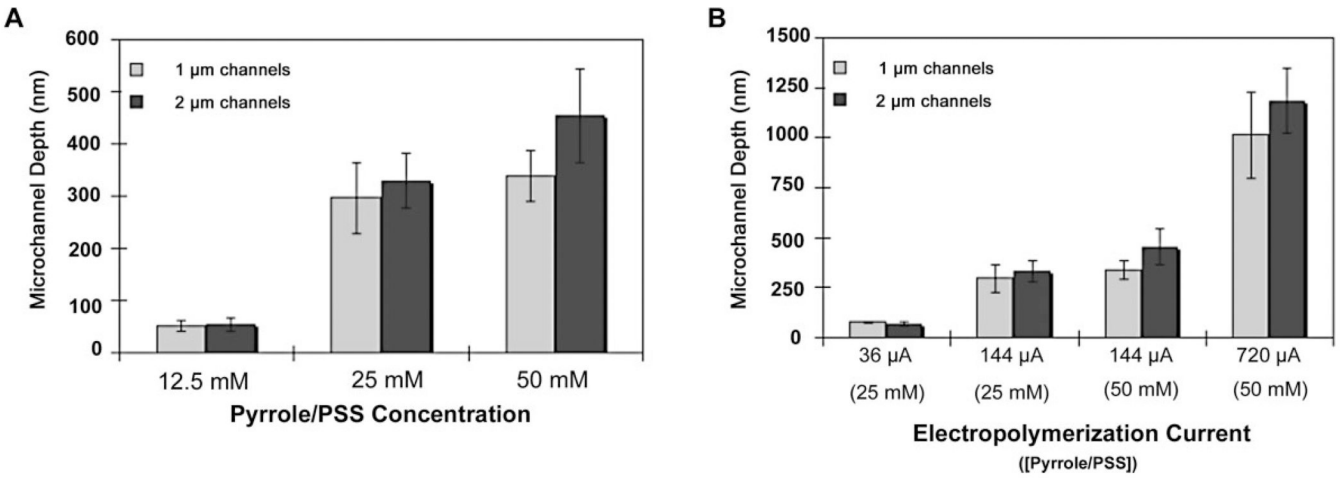

Figure 3.

The effect of pyrrole/PSS concentration and electropolymerization current on PPy microchannel depth. A) The depth of microchannels polymerized with 144 μA, 30 s polymerization time, and increasing monomer/dopant concentration; B) the depth of microchannels polymerized with two different concentrations (25 or 50 mM pyrrole/PSS concentration), 30 s of polymerization time, and increasing current. The combination of higher concentration (50 mM) and current (720 μA) produces a very significant increase in depth. Error bars represent the STET.

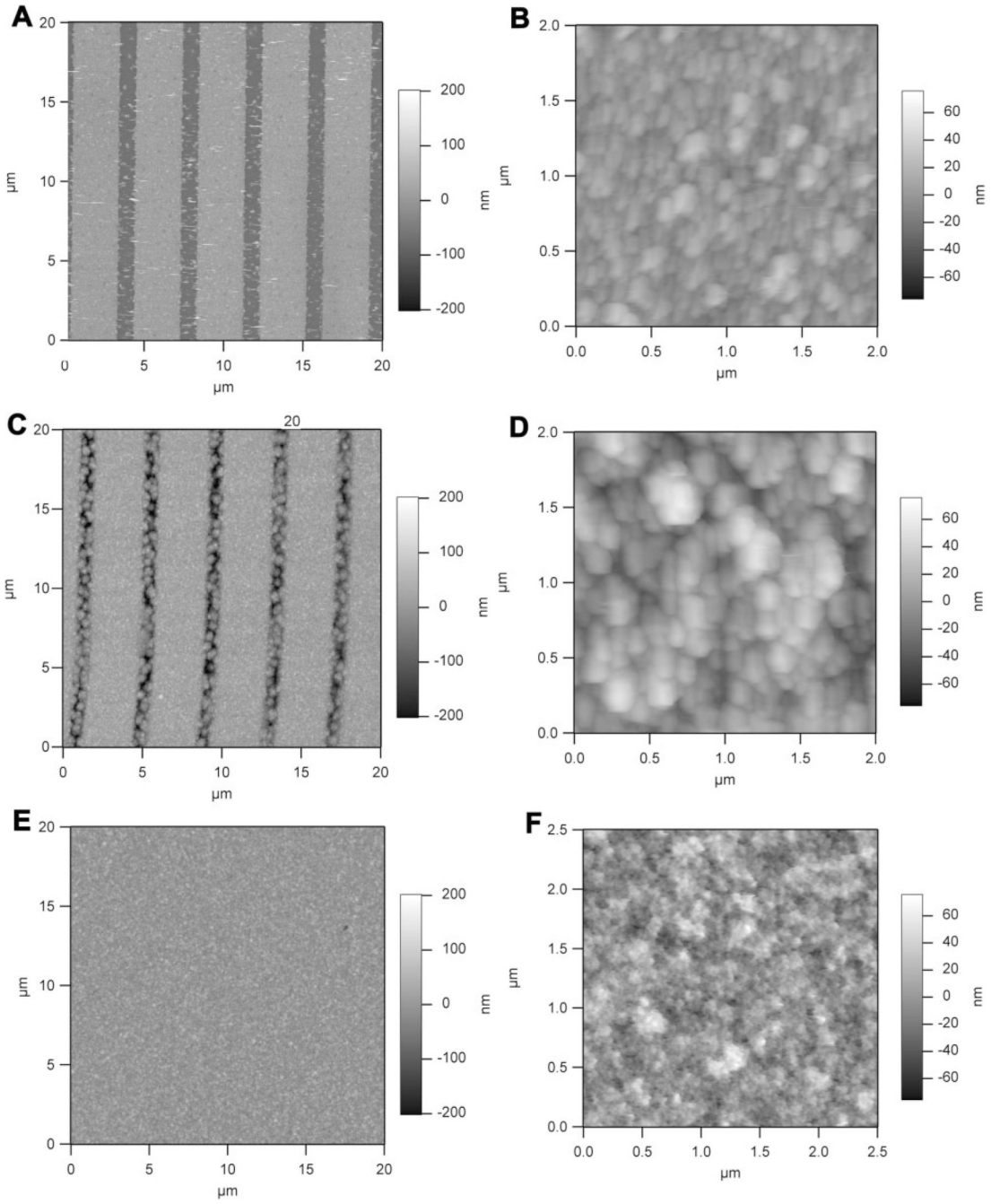

Figure 4.

Representative AFM images of PPy microchannels. A) A 20 µm × 20 µm scan of PPy microchannels synthesized with 12.5 mM pyrrole/PSS, 144 µA polymerization current, and 30 s of polymerization time; B) a 2 µm × 2 µm scan of a PPy microchannel ridge with the same conditions as in (A) (root mean square (rms) = 10.79 ± 1.04 nm); C) a 20 µm × 20 µm scan of PPy microchannels synthesized with 50 mM pyrrole/PSS, 720 µA polymerization current, and 30 s of polymerization time; D) a 2 µm × 2 µm scan of PPy microchannels with the same conditions as in (C) (rms = 20.45 ± 1.78 nm); E) a 20 µm × 20 µm scan of PPy thin film synthesized with 25 mM pyrrole/PSS, 7200 µA polymerization current, and 60 s of polymerization time; F) a 2 µm × 2 µm scan of PPy microchannels with same conditions as in

(E) (rms = 19.25 ± 2.28 nm). Higher monomer/dopant concentration and larger polymerization current increased the PPy microchannel roughness.

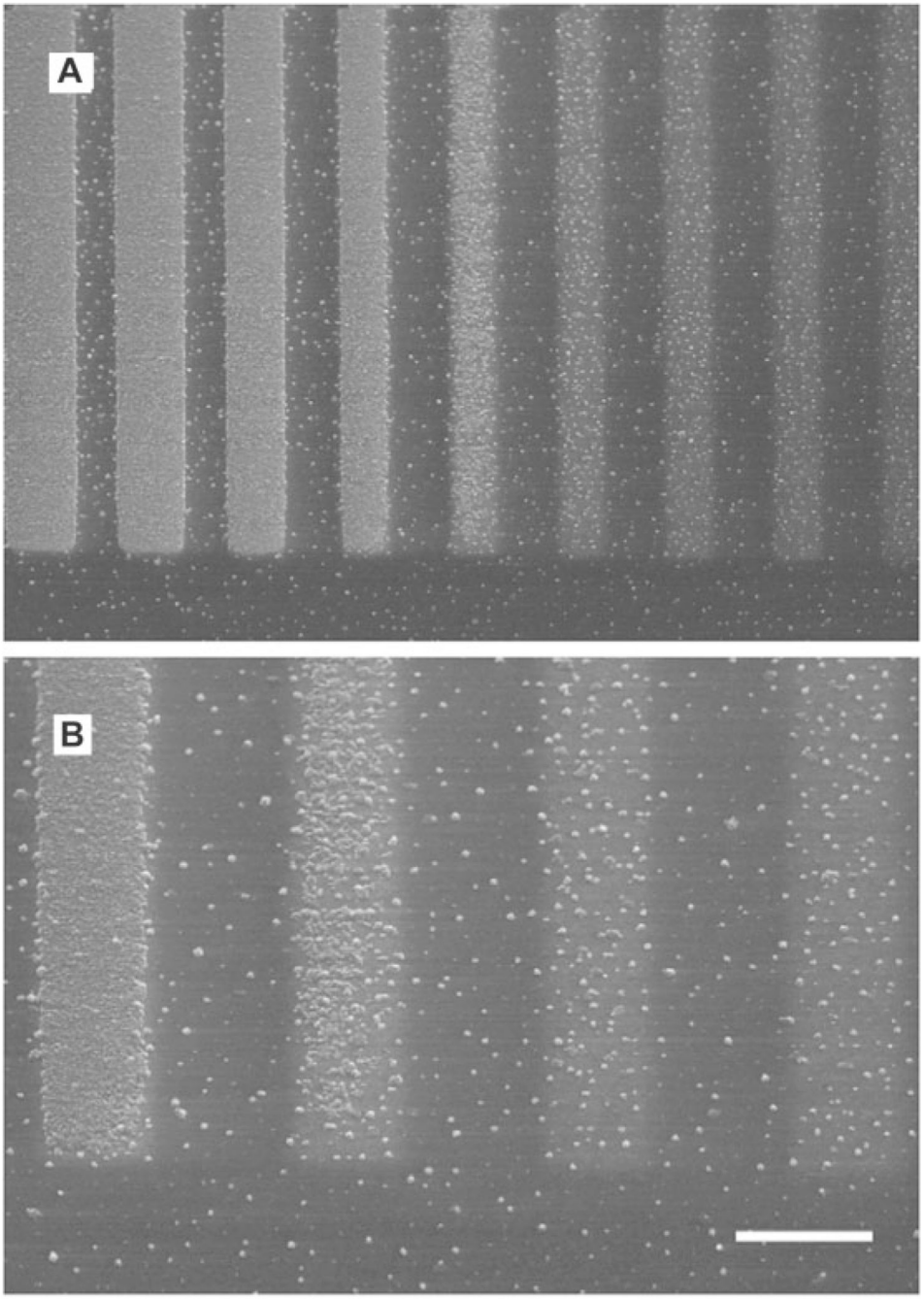

Figure 5.
SEM microscopy images of microchannels written with different e-beam currents. A) Microchannels written with a decreasing current ramping from 0.16 nA (left side of image) to 0.02 nA (right side of image), and polymerized with 25 mM pyrrole/PSS concentration, 144 μA polymerization current, and 30 s of polymerization time; B) a higher-magnification image of microchannels with different PPy thickness. Higher e-beam currents produced deeper and more defined patterns. The scale bar is 5 μm (A) and 2 μm (B).

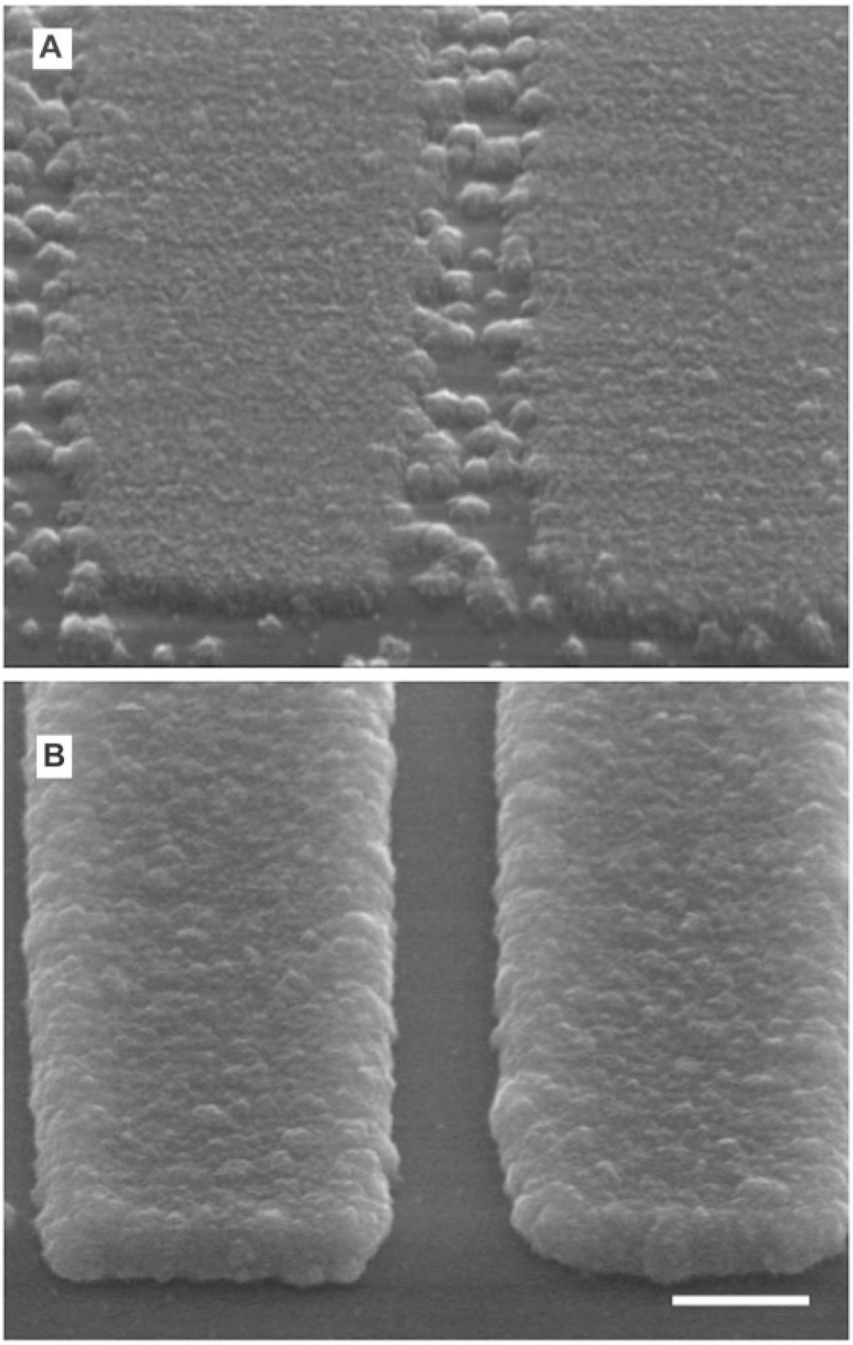

Figure 6.
SEM microscopy images of microchannels written on different resist thicknesses. A) Microchannels polymerized on a PMMA resist ca. 10 nm thick with 50 mM pyrrole/PSS concentration, 144 μA, and 30 s (microchannel depth = 338 ± 49 nm); B) microchannels polymerized on a PMMA resist ca. 100 nm thick with 50 mM pyrrole/PSS concentration, 144 μA, and 30 s (microchannel depth = 799.3 ± 113 nm). Thicker resist produces deeper and more defined microchannels. The scale bar is 1 μm. Images are at the same magnification.

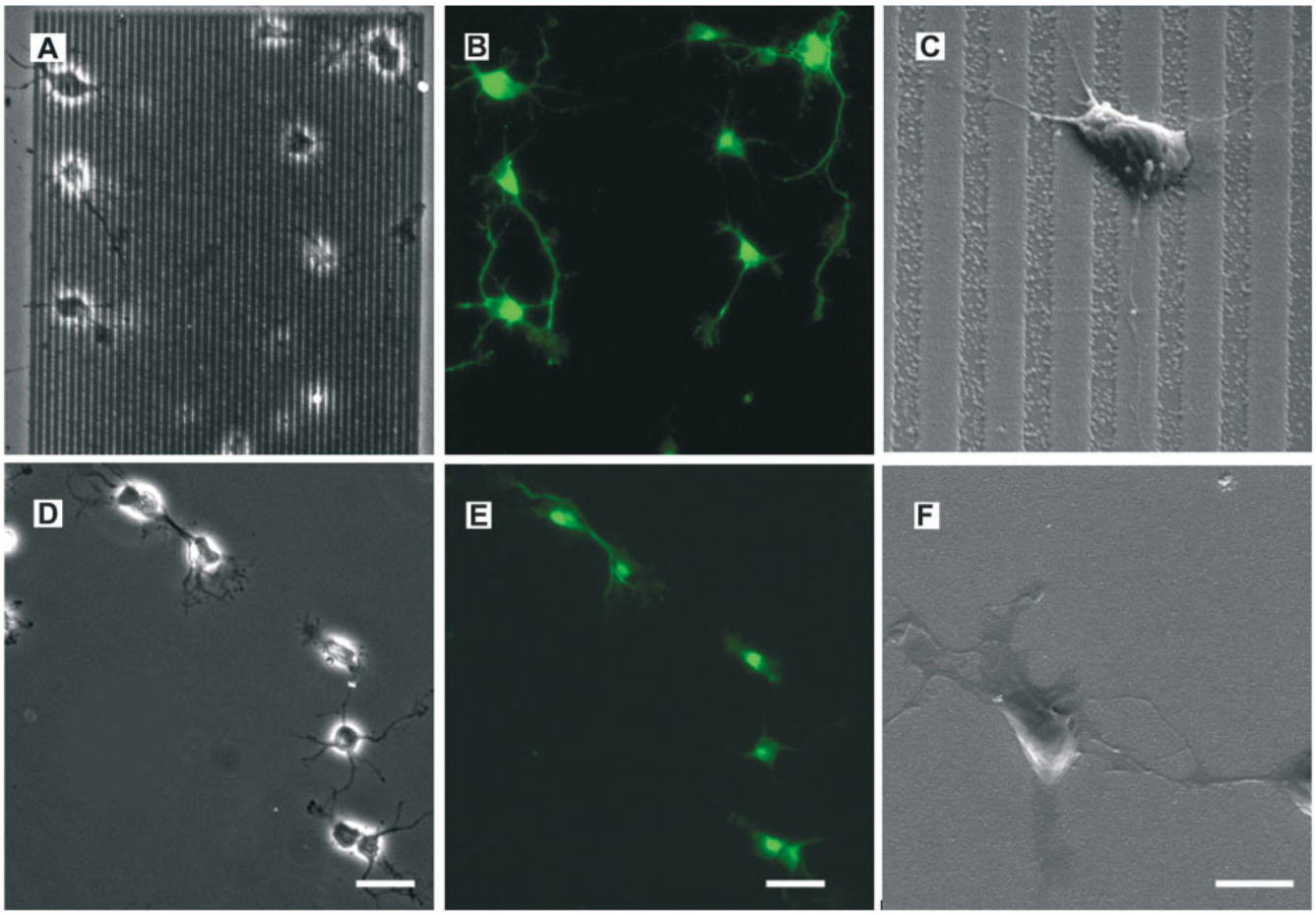

Figure 7.

From left to right: phase-contrast, fluorescence, and SEM microscopy images, of hippocampal neurons on PPy. A–C) Cells cultured on 2 μm wide and 200 nm deep PPy microchannels; D–F) cells cultured on unmodified PPy. The green labeling (Alexa 488) corresponds to Tau-1 (axonal marker) immunostaining. Cells polarized more readily on microchannels than on unmodified PPy. The scale bar is 20 μm (A,B,D,E) and 5 μm (C,F).

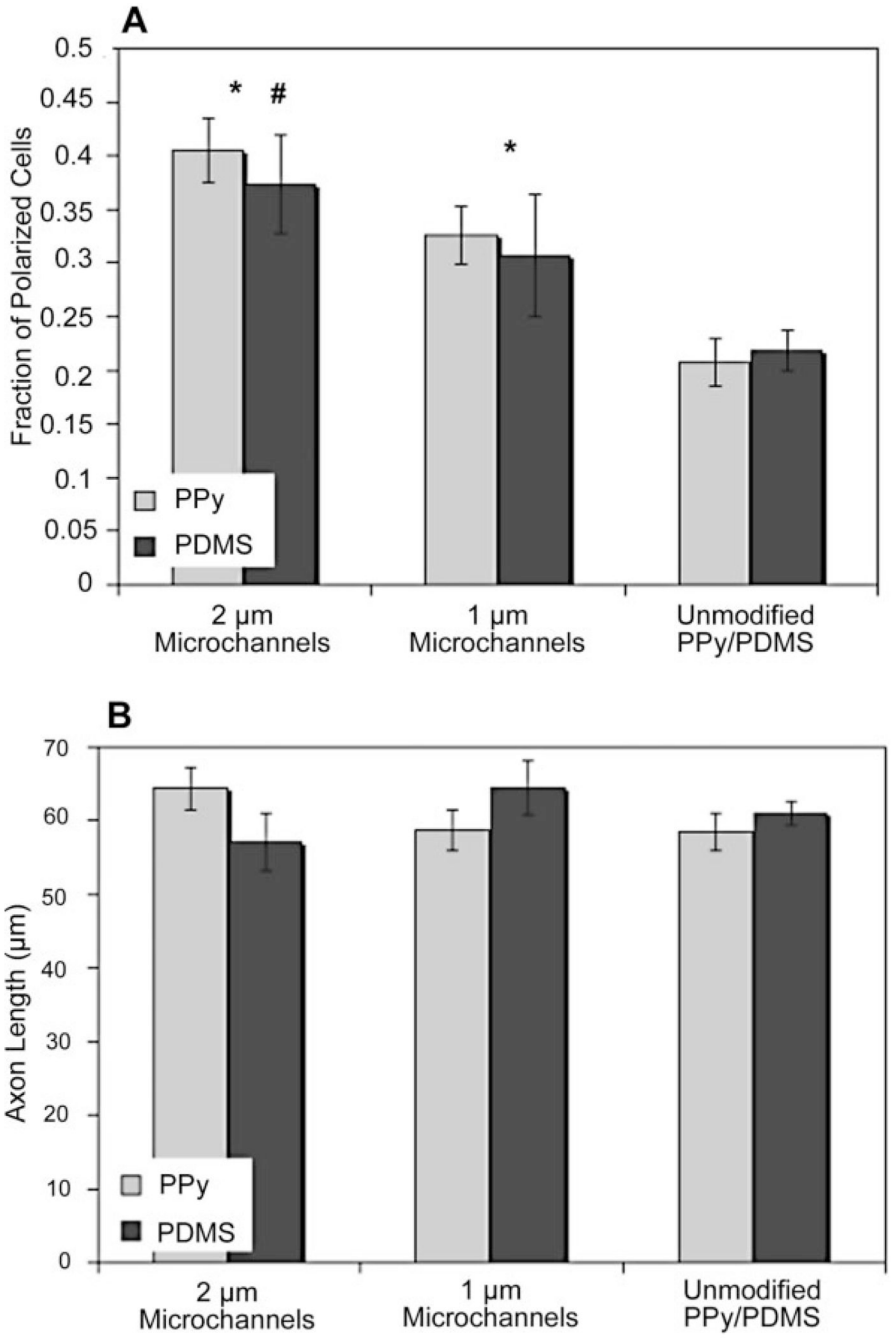

Figure 8.

Quantitative analysis of neuron polarization and axon length. A) The fraction of neurons with defined axons after 20 h in culture (n = 5 experiments with ca. 100 neurons analyzed per experiment) on PPy or PDMS substrates; B) axon length of polarized cells on PPy or PDMS substrates. The error bars correspond to sem. Topography increased polarization but not axon growth. The symbols * and # represent statistically significant differences from unmodified PPy/PDMS and 1 µm microchannels, respectively, using a t-test with probability $P < 0.05$.

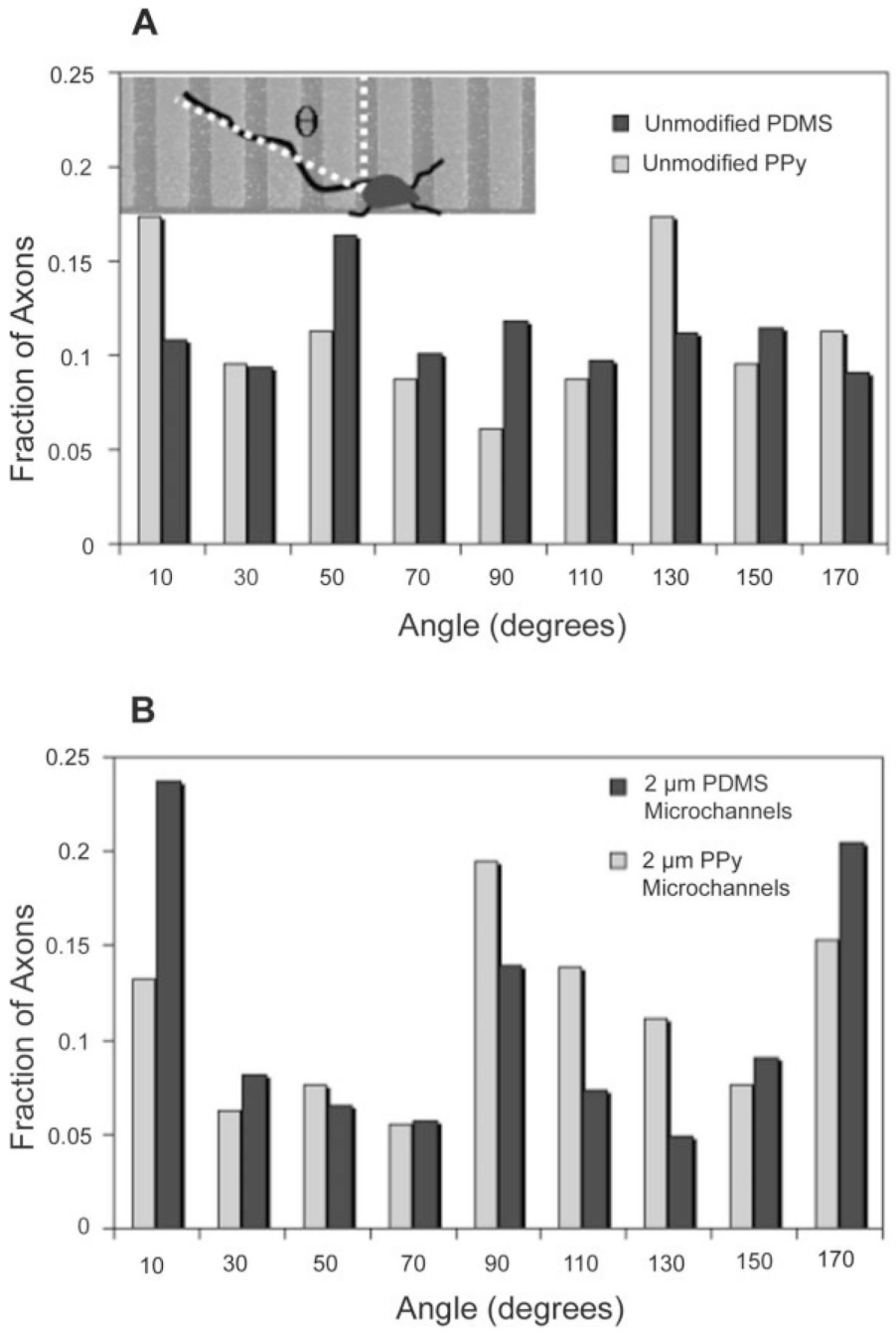

Figure 9.

A quantitative analysis of the axon angle. Histograms for axon angle distribution on A) unmodified PPy/PDMS substrates and B) 2 μm PPy/PDMS microchannels. The angle was measured as illustrated in the inset. Neurons extended axons in parallel or perpendicular orientations to the microchannels on both materials, but the fraction of axons growing parallel to PPy microchannels was lower than the fraction on PDMS microchannels.

Table 1

Electropolymerization conditions and microchannel depth, gap width and roughness.

Polymerization Conditions			Microchannel Depth [nm] [a]		Microchannel Gap Width [nm] [b]		RMS Roughness [nm] [c]
Pyrrole / PSS [mM]	Current [μA]	Time [seconds]	2 μm	1 μm	2 μm	1 μm	
12.5	144	30	54.1 ± 12.9	51.0 ± 10.5	14310.0 ± 70.0	468.8 ± 17.3	10.79 ± 1.04
25	36	30	68.8 ± 11.4	78.8 ± 3.7	1197.3 ± 110.4	274.3 ± 111.9	11.74 ± 0.26
25	144	10	275.2 ± 14.8	241.9 ± 36.0	1059.7 ± 114.8	314.2 ± 181.9	13.66 ± 0.18
25	144	30	329.4 ± 53.4	296.5 ± 68.1	988.0 ± 125.1	147.0 ± 79.5	14.27 ± 0.38
50	144	30	454.6 ± 89.5	338.7 ± 49.0	202.0 ± 202.0	37.3 ± 37.3	15.06 ± 0.29
50	720	30	1184.1 ±161.2	1012.3 ± 214.5	0	0	20.45 ± 1.78
100	720	30	2134.4 ±500.0	1628.8 ± 378.5	0	0	33.55 ± 0.71
				PPy Thin Films (Controls)			
25	7200 [d]	120	N/A	N/A	N/A	N/A	19.25 ± 2.28

[a] Obtained from cross-sectional scanning electron microscopy (SEM) images for $n = 3$ samples (average ± standard error in the mean (sem)).

[b] Obtained from cross-sectional SEM images for $n = 3$ samples (average ± sem); the width was measured at the bottom section of the gap.

[c] Obtained from atomic force microscopy (AFM) images for $n = 3$ areas of a representative sample (average ± sem).

[d] Higher current and time were required because of larger polymerization areas.